



Cooling channel free surface optimisation for additively manufactured casting tools

Tongyan Zeng¹ · Essam Abo-Serie² · Manus Henry¹ · James Jewkes²

Received: 6 February 2023 / Accepted: 4 April 2023 / Published online: 26 May 2023
© The Author(s) 2023

Abstract

In the present study, an algorithm has been developed using the adjoint method to optimise the position and cross-section of an internal cooling channel for a 3D printed tool steel insert for use in the aluminium die-casting process. The algorithm enables the development of an optimised complex industrial mould with relatively low computational cost. A transient model is validated against multiple experimental trials, providing an adapted interface heat transfer coefficient. A steady state thermal model, based on the casting cycle and thermal behaviour at the mould surface, is developed to evaluate the spatial distribution of temperature and to serve as the initial solution for the subsequent optimisation stage. The adjoint model is then applied to optimise the cooling channel emphasising the minimisation of the temperature standard deviation for the mould surface. The original transient model is applied to the optimised mould configuration via calibration using experimental data obtained from a dedicated aluminium furnace. The optimised cooling channel geometry, which uses a non-uniform cross-section across the entire pipe surface region, improves the pressure drop and cooling uniformity across the mould/cast interface by 24.2% and 31.6%, respectively. The model has been used to optimise cooling channels for a range of industrial high-pressure aluminium die-casting (HPADC) inserts. This has yielded a significant improvement in the mould operational lifetime, rising to almost 130,000 shots compared to 40,000 shots for prior designs.

Keywords Adjoint optimisation · Aluminium high-pressure die-cooling · Conformal cooling · Die cooling optimisation

1 Introduction

Injection moulding and die-casting are well-established manufacturing fields that are receiving renewed attention due to the design opportunities arising from the development of additive manufacturing (AM) methods. These novel AM technologies are uninhibited by the shape limitations imposed by conventional computer numerical

control (CNC) machining methods, enabling the creation of complex internal voids, such as conformal cooling channel layouts [51]. This capability supports the design of conformal passages in mould inserts to maximise thermal performance [1–4]. Die-casting processes, such as gravity and high-pressure die-casting (HPDC), share some similar features with plastic injection moulding, including material injection, cooling, and part ejection. However, metal tool casting entails more extreme operating conditions than for polymer injection moulding, requiring further developments in the understanding of the physical and cooling processes. Nevertheless, some design/optimisation concepts from plastic injection moulding may have potential value in die-casting applications. Key challenges within die-casting processes include non-uniform thermal distributions, high-temperature gradients, and excessive boundary heat-flux variations at the mould/cast interface. These factors can cause undesirable effects such as product shrinkage, warpage, and thermal residual stresses, which can influence the total cooling time and part quality [5, 6]. Accordingly, the development of an optimal cooling

✉ James Jewkes
jwj5@leicester.ac.uk

Tongyan Zeng
zengt5@uni.coventry.ac.uk

Essam Abo-Serie
e.aboserie@leicester.ac.uk

Manus Henry
ad4507@coventry.ac.uk

¹ Centre of Fluid and Complex Systems, Coventry University, Coventry CV1 2NL, UK

² School of Engineering, University of Leicester, Leicester LE1 7RH, UK

channel layout for a rapid-prototyped mould insert is of considerable interest to the industry.

Optimisation strategies for AM casting tools include external and internal approaches. Developments in external optimisation include advanced rapid tooling (RT) techniques such as direct metal laser sintering (DMLS), also known as SLS, stereo-lithography (SLA), and powder bed fusion (PBF) [7, 8]. Additional innovations include replacing the mould cast with high thermal conductive material or alloys [9, 10] or adding an intermediate layer between cavities [11, 12]. These studies all demonstrate improvements in the thermal efficiency and/or mechanical performance of the finished injection mould. Adding lubrication and spraying processes can also help to achieve more uniform cooling for the demoulding process [36]. However, control of the lubricant spray is a challenging task when targeting specific die surfaces and is commonly treated as a separate operation applied between injection cycles. It is therefore not considered here as part of the cast modelling process despite its 20–50% contribution to cooling in older HPDC systems [37].

While external optimisation is still limited by the manufacturing process and material type, optimisation of the internal cooling passage design remains the most widely used and effective approach for injection moulding development [14]. Here, parameterisation studies are widespread especially with the development of AM technology. Depending on the specification of the casting material and part complexity, different design parameters may be considered, such as the number of cooling channels, pipe diameter, pitch, distance between parallel pipes, and the depth between channels/casting surface [49]. For example, [29] describes a casting die-design which minimises cooling time by consideration of cooling channel number, location, and flow rate. The inclusion of extra structures, such as internal baffles or lattices, or secondary cooling layers, can also be beneficial [16]. The conventional circular cross-section channel geometry has been used in the majority of cooling design cases, in order to avoid overheating around the corner or sharp edges. However, more advanced studies have demonstrated improved performance through the adoption of alternative cross-sectional geometries [48]. An aluminium-filled epoxy injection mould tool study [14], using a profiled cross-section, achieved an 18% reduction in cooling time [14]. Another design using grooved square and rectangular channel geometries improved cooling time and warpage by up to 65% and 54%, respectively [15]. Although various non-circular geometries have been proposed, the cross-sectional profile has generally been kept constant, and there has been very little research reported into the use of non-uniform cross-sectional profiles for conformal cooling channels in injection moulds.

The idea of using a non-uniform cross-section profile can be linked to the study of the response surface methodology (RSM). The adjoint method is a powerful numerical approach used to calculate a predefined mesh sensitivity based on a selected objective function. This concept was initially developed by Lions and Pironneau [17, 18] in the 1970s and was further developed by Jameson [19, 20] who pioneered its use in the field of aeronautical computational fluid dynamics. By the mid-1980s, aerodynamic flow simulations were conducted using more complicated Euler and Navier–Stokes equations [21, 22]. The adjoint method offers independence between computational cost and the number of design variables, making it a useful tool for problems with large design spaces. Studies based on the adjoint method can be divided into two main categories: topology optimisation and surface deformation optimisation. Topology optimisation generates the surface mesh based on predefined constraints for each cell within a specified domain, whereas surface deformation optimisation morphs a predefined surface mesh from a baseline design. Both methods require a surface sensitivity analysis provided by a gradient-based adjoint method. Currently, the topology approach is used to design both basic elements and more complex geometries for conformal cooling systems in injection moulding applications and has delivered improved pressure drop, thermal efficiency, and uniformity [23–25, 52]. The adjoint surface deformation method remains under-explored in the domain of injection moulding and die-casting tools. One study utilised this approach to maximise heat transfer and reduce cooling cycle time for a zinc alloy pressurised die-casting process [26]. The resulting design featured a non-uniform profile region for a cooling pipe and achieved a 60% reduction in cycle time despite poorly manufactured optimisation surfaces. The main challenges to further develop this approach are the extreme thermal operation conditions, complex interfacial heat transfer relationships, and the availability of commercial computational power.

The heat transfer behaviour during the early stages of the aluminium die-casting process has a high impact on the quality of the final casting. At the beginning of the casting process when molten aluminium is in close contact with the mould surface, the heat transfer rate between the two media is at its highest value. Once a small void region forms between the mould and the cast, caused by the shrinkage of the rapid cooling metal, the heat transfer rate drops, affecting the thermal resistance and solidification rate. Accordingly, the interface heat transfer coefficient (IHTC) varies both in space and time across the mould/cast interface. Parameters influencing the IHTC addressed in previous studies include mould temperature, contact pressure, material specification, surface finishing roughness, and coating [39–41]. For gravity die-casting, several approaches have been used to determine the IHTC throughout the casting cycle [39, 41,

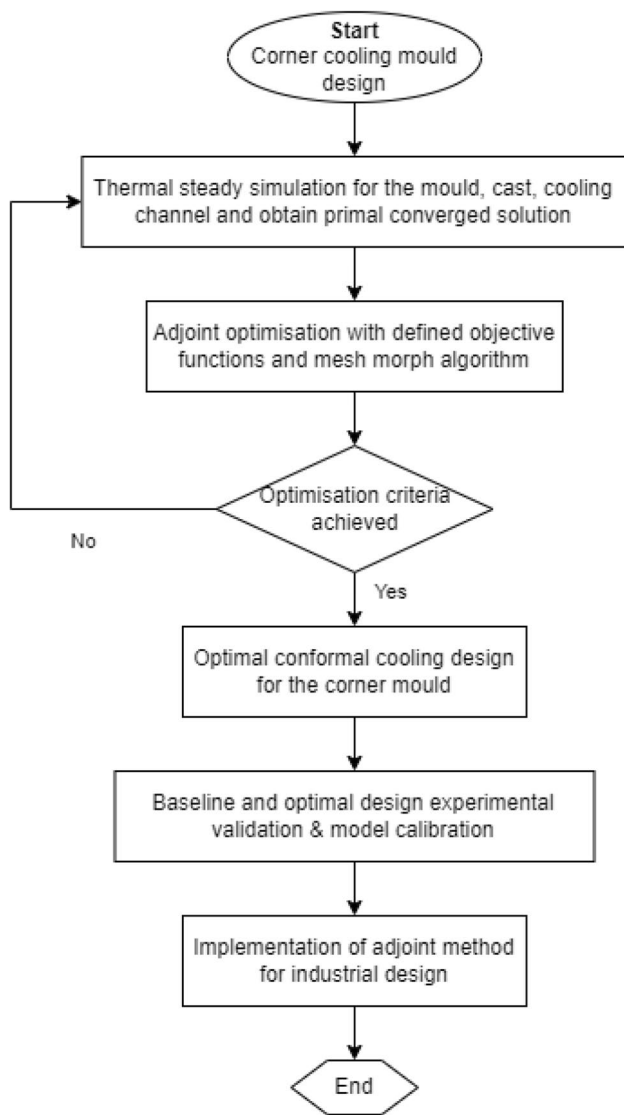


Fig. 1 Adjoint optimisation flow chart for the corner baseline mould

42]. The most developed model focuses on evaluating the thickness of the coating layer and air gap generated by thermal extraction [40]. Most of these studies show good agreement with their experimental validation, whereby for the majority of the monitoring points the IHTC settles to an almost constant value during the casting cycle. However, such agreement depends on the design configuration and material specification. One finite element study suggests a range of 3500–7000 W/m² K for the IHTC in a permanent mould casting process [31]. For high-pressure aluminium die-casting (HPADC), researchers have observed a high value of approximately 130 kW m⁻² K⁻¹ [43] for the IHTC at the beginning of the injection process, dropping significantly within a few seconds to an almost constant value of between 2 and 3 kW m⁻² K⁻¹ [38]. Given the impact of the dynamic IHTC in the aluminium die-casting process, it is important

to obtain good agreement, or calibration, between numerical simulations and experimental results for this parameter.

In the present work, we introduce the adjoint surface deformation method to optimise a baseline corner cooling design for aluminium die-casting, simulated using STAR-CCM+ [44]. The objective function is designed to deliver both uniform cooling at the mould/cast interface and minimal pressure drops across the cooling channel. A second, fully developed thermal model and design procedure is described which simulates the manufacturing process in more detail. Further sections describe the final optimal configuration of the corner design for the aluminium die-casting process, the calibration of the thermal model against experimental data, the limitations of our approach, and future challenges. For the industrial complex model, and to reduce the computation cost, the fluid flow in the cooling channels has been simulated separately, and the interface heat transfer coefficient has been determined and then mapped to the mould surfaces.

2 Methodology

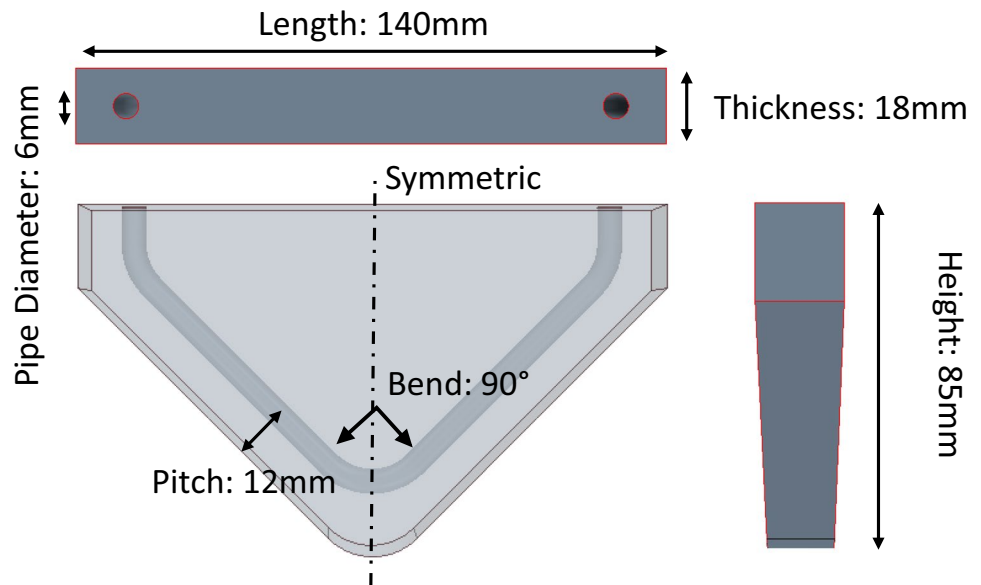
This study develops a methodology to optimise the cooling channels for casting inserts which is applied to develop a basic corner geometry. In outline, the process for developing the baseline design is shown in Fig. 1. The optimisation process begins by developing a steady thermal model for the aluminium die-casting process, including all solvers, boundary conditions, and assumptions. Having obtained a well-converged primal solution for the baseline cooling channel design, the adjoint model is implemented to optimise the corner design case with the mesh morph algorithm applied using the two objective parameters. Once all defined stopping criteria are met, the optimal cooling channel geometry for the basic element is obtained.

The second part of this study describes testing and calibrating the optimal cooling design results against experiment. Experimental evaluation is conducted on both the baseline and optimal design of the corner cooling design to provide a final calibration of the cast/mould IHTC between the aluminium cast and steel mould for the whole casting cycle. Lastly, the resulting adjoint optimisation method is implemented to optimise a complex industrial HPDC tool, where only the mould surface cooling uniformity is considered.

2.1 CFD model

The CFD model of the aluminium die-casting process is presented in this section. This uses a simulation model for the steady-state condition followed by an adjoint model with

Fig. 2 Baseline design of the corner channel for furnace test-rig



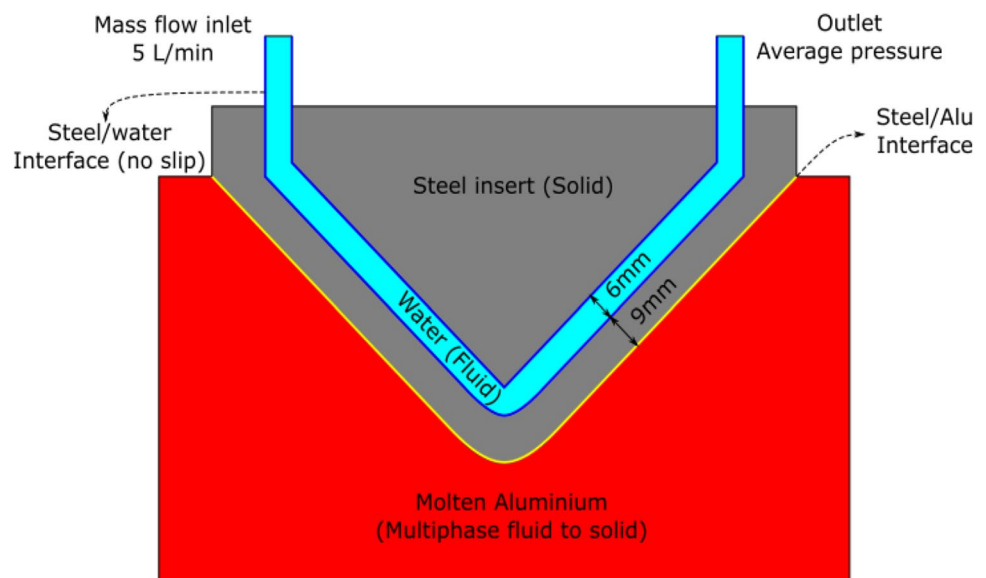
dual objective functions. The associated mesh-morphing algorithm and the transient model for calibration against experimental data are then described. This simplified algorithm minimises computational time without sacrificing quality or accuracy.

2.1.1 Model geometry

The basic cooling pipe geometry selected as the case study is a corner, where the challenge is to achieve uniform cooling. This is shown in Fig. 2 with dimensions 140 mm length and 18 mm thickness. The baseline parameters for the single cooling channel match industrial standards, adopting a uniform 6 mm channel diameter and a

constant 12 mm pitch distance to the bottom surface, which is in contact with the molten aluminium. The baseline model of the aluminium die-casting process is divided into three regions as shown in Fig. 3: molten aluminium cast (red), 3-D printed tool steel (grey), and cooling passage/water coolant (blue). There are two contact interface planes: between the molten aluminium and the mould, and between the mould and the cooling channel. The adiabatic boundary condition is applied to the remaining external faces of the solid steel region, and a no-slip condition is applied to the walls of the cooling channel with a 0.3 mm surface roughness, based on the measurements of average roughness R_a and peak-valley difference R_z of the 3-D printed pieces.

Fig. 3 Steady model with highlighted regions and BDs



The basic element corner design is discretised using polyhedral cells, and a mesh-convergence study is carried out to ensure that the results are independent of mesh resolution. The base size of the mesh in the solid and fluid regions is set as 0.005 m and 0.0025 m, respectively. The total entity count of the number of cells for the corner design is 166,576. The mesh quality is evaluated based on the mesh validity, skewness angle, and volume change ratio [45] which gives an overall mesh quality of 97.9%. When solving the near-wall viscous transitional sublayer, the all-Y+ wall treatment model enables characterised mesh densities between different boundary layers. By adapting the finite control volume package STARCCM+, the Prism layer is also activated on the walls and interfaces to accurately calculate the heat flux.

2.1.2 Steady model for optimisation

A steady flow model is developed to simulate the coolant inside the pipe for the aluminium die-casting process for this study. The cast part is considered as a heat source, and the volumetric heat generation is evaluated based on the solidification energy over the entire casting cycle. This steady model also acts as the first stage of optimisation for the baseline design, which is followed by surface optimisation using the adjoint method. The Reynolds-Averaged Navier–Stokes (RANS) turbulence model is used to solve the coolant fluid in the channels with the governing equations of fluid flow mass and momentum and energy:

$$\nabla \cdot (\rho \bar{\mathbf{v}}) = 0 \quad (1)$$

$$\nabla \cdot (\rho \bar{\mathbf{v}} \otimes \bar{\mathbf{v}}) = -\nabla \cdot \bar{\mathbf{p}} \mathbf{I} \quad (2)$$

$$\nabla \cdot (\rho \bar{\mathbf{E}} \bar{\mathbf{v}}) = -\nabla \cdot \bar{\mathbf{p}} \bar{\mathbf{v}} - \nabla \cdot \bar{\mathbf{q}} \quad (3)$$

where ρ is the fluid density, $\bar{\mathbf{v}}$, $\bar{\mathbf{p}}$, $\bar{\mathbf{E}}$, and $\bar{\mathbf{q}}$ are the mean velocity, pressure, the total energy per unit mass, and heat flux, respectively, and \mathbf{I} is the identity tensor. A K-Omega shear-stress transport (SST Menter [28]) turbulence closure is used for the turbulent water regions with Reynolds Number higher than 6000, as it provides better prediction of flow separation and good performance in pressure gradients, as well as avoiding the problem of sensitivity for free stream/inlet conditions. Uniform mass flux is applied at the pipe inlet with a constant volume-flow rate of 5 L/min (equivalent to 2.94 m/s fluid velocity). The initial coolant temperature is set to 70 °C, matching industrial practice. To ensure a fully developed inlet flow, the inlet pipe is extended outside the mould by 5D, i.e. 30 mm. A coupled implicit solver supports the use of the adjoint solver to simulate both the solid and fluid regions. The material specifications of the H13 mould steel, A380.0-F die casting alloy and water coolant are provided in Table 1.

Basic conduction and convection equations are implemented to solve the heat transfer between the aluminium cast, steel mould, and water. A conjugate heat transfer (CHT) model is used to solve the conductive and convective energy equations between the three regions. Fourier's law of conductive heat transfer between the solid mould and cast regions can be written as

$$\mathbf{q}_s = -k \nabla T \quad (4)$$

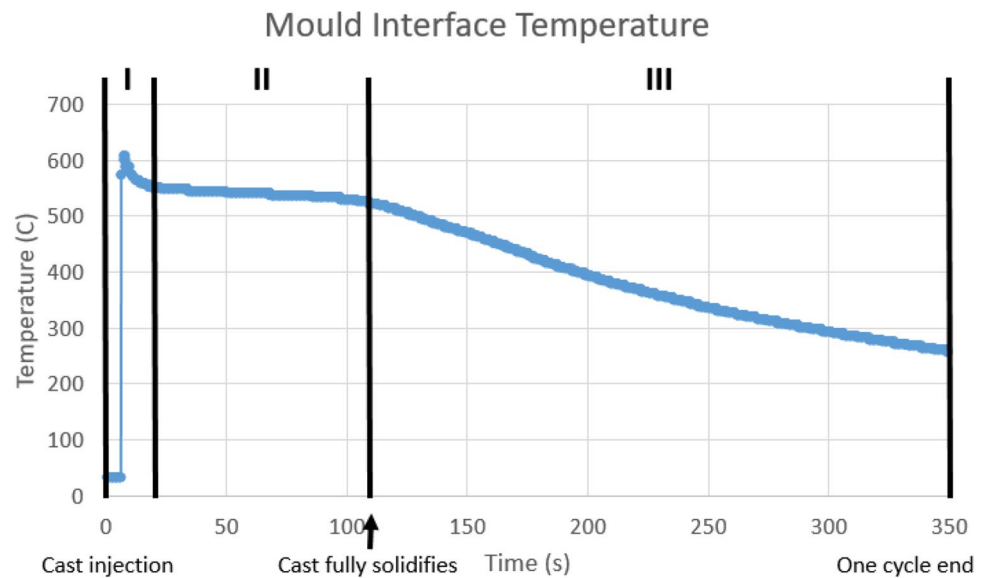
where the heat thermal conductivity k and difference in temperature are readily obtained. The average heat flux at the interface is dependent on many factors including the volume of the cast, cast thickness, and pipe depth/location. Initial close contact between the cast aluminium and steel mould leads to high values for the initial interface heat flux. However, this drops rapidly (depending on the location of the coolant channel) and reaches an almost constant value until the cast fully solidifies. This is illustrated in the three-phase mould interface temperature plot in Fig. 4 derived from experimental data collected over a typical industrial cycle. Accordingly, the steady model is based on phase two of the casting process.

To extend the duration of phase 2 and thereby provide a longer period to calibration the IHTC coefficient, the initial aluminium melt temperature is set at a high value of 750 °C in both simulation and experiment. While this is not representative of conventional industrial practice, it has been helpful in supporting the analysis and optimisation required to achieve interfacial thermal uniform cooling. The hot aluminium cast is treated as an energy source providing heat flux with constant

Table 1 Material specifications

| EN AC-46000 (46,000-F, AlSi9Cu3(Fe)) cast aluminium [33] | |
|--|------------------------|
| Density | 2760 kg/m ³ |
| Specific heat | 963 J/kg K |
| Thermal conductivity | 130 W/m-K |
| Dynamic viscosity | 0.00125 Pa. s |
| Latent heat of fusion | 3.89e5 J/kg |
| Initial temperature | 650 °C |
| Casting solidus temperature | 538 °C |
| Casting liquidus temperature | 593 °C |
| Casting injection temperature | 650 °C |
| Tool steel, H13 [34] | |
| Density | 7750 kg/m ³ |
| Min specific heat | 587 J/kg-K @ 300 K |
| Max specific heat | 777 J/kg-K @ 700 K |
| Min thermal conductivity | 24.86 W/m-K @ 300 K |
| Max thermal conductivity | 28.7 W/m-K @ 700 K |
| Initial temperature | 200 °C |
| Others | |
| Average roughness Ra | 300 µm |
| Peak-valley difference Rz | 10,600 µm |

Fig. 4 Mould interface thermal variation over one casting cycle



average volumetric heat generation over the entire cycle. This energy \dot{Q} can be expressed by the following equation:

$$\dot{Q} = \frac{\rho[h_{fs} + Cp_{Al,s}(T_s - T_{demold}) + Cp_{Al,l}(T_{melt} - T_L)]}{t_{cycle}} \quad (5)$$

$Cp_{Al,s}$ and $Cp_{Al,l}$ represent the specific heat of the solid and liquid aluminium phases, while the solidus and liquidus temperature of the cast part are T_s and T_L , respectively, and t_{cycle} is the cycle time. The demoulding temperature is 450 °C based on industrial practice. The heat generated at each cell within the cast domain is evaluated from Eq. 5 multiplied by the cell volume. The total heat transfer from the cast region is the same as the heat received from the mould then convectively dissipated to the coolant channel.

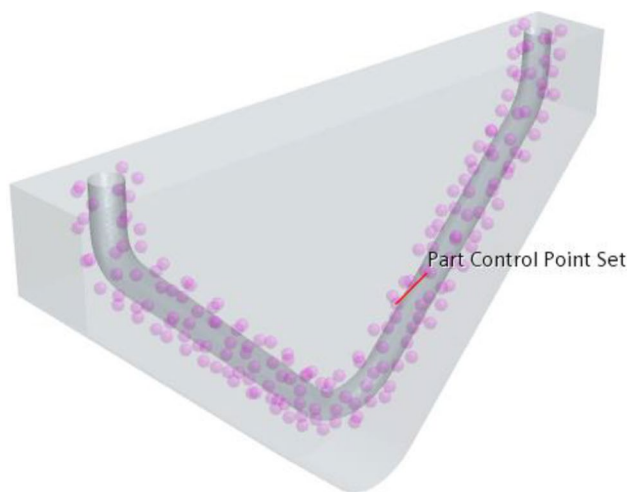


Fig. 5 Control point-set around the morph cooling surface

2.1.3 Adjoint cost functions and mesh morph algorithm

Our first targeted adjoint cost function J_1 minimises the temperature standard deviation of the mould/cast interface at the mould side. The second cost function J_2 minimises the pressure difference between the inlet (high-pressure) and exit (low-pressure) coolant channel at the boundary surfaces:

$$\text{Pressure drop } J_2 = \left[\frac{\sum_f P_f A_f}{\sum_f A_f} \right]_H - \left[\frac{\sum_f P_f A_f}{\sum_f A_f} \right]_L \quad (6)$$

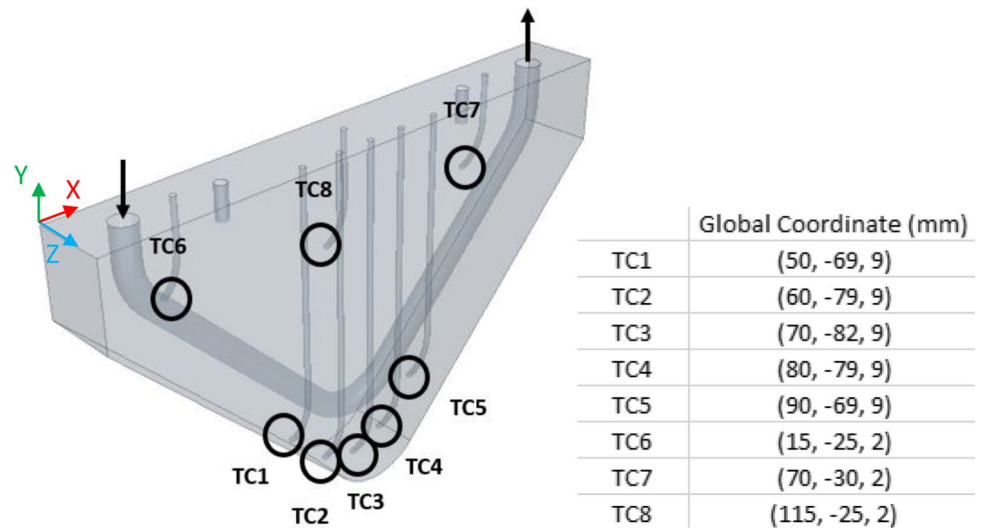
The adjoint method predicts the influence of different input parameters or quantities of interest. It calculates the sensitivity of the objective function with respect to input parameters which may be design variables or values at the boundary conditions. By changing cell location not only will the channel location change but also an arbitrary cross-sectional geometry can be generated along the channel. Each of the objective cost functions associated with the flow-field variables U and the control point of body x can be written as

$$J = J(U(x), x) \quad (7)$$

Optimisation requires the gradient of the objective function for minimisation and is dependent on both design variable and flow field variables $J(U(x), x)$. It is subject to the constraint of the discrete governing equations (Navier–Stokes) $R(U(x), x) = 0$ which can be rewritten as

$$\frac{dJ}{dx_k} = \frac{\partial J}{\partial U} \frac{dU}{dx_k} + \frac{\partial J}{\partial x_k} \quad (8)$$

Fig. 6 Thermocouple insert locations for corner baseline design



and which is subject to the following constraint:

$$\frac{\partial R}{\partial U} \frac{dU}{dx_k} + \frac{\partial R}{\partial x_k} = 0 \quad (9)$$

The RBF interpolation approach is used to define the design variables, and the adjoint solver uses the RBF equation to deform the mesh. There is no mesh dependency for the RBF method which means the same interpolation solution can be applied to multiple meshes by reading results at different node locations [46, 47]. Being a meshless method

also allows grid points to be moved regardless of which elements are connected to them and so it is suitable for parallel implementation.

A control points group consisting of 180 nodes is generated with a 2 mm equal separation and 5 mm off-set distance above the cooling surface, as shown in Fig. 5. These points, together with the local mesh coordinates, define the movement on both the boundary and the interior mesh. All control points are free of movement without displacement constraints; nevertheless, the new positions of control points



Fig. 7 Experimental setup for the corner mould design

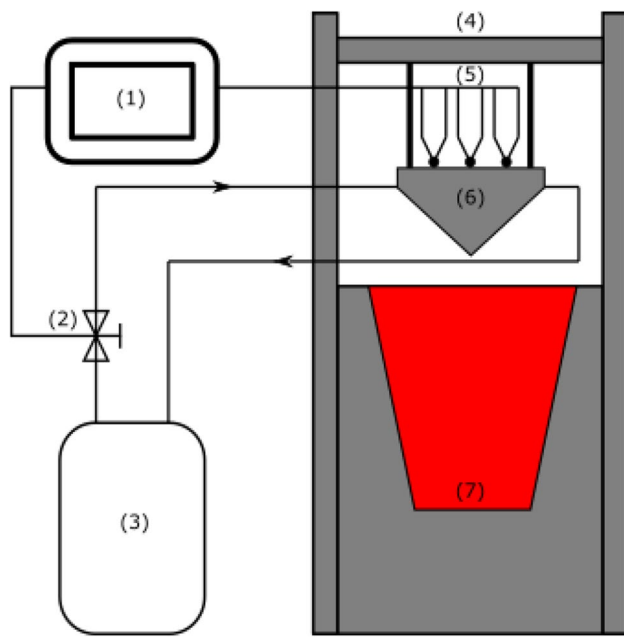


Fig. 8 General diagram of furnace experimental setup. (1) Data logger. (2) Flow rate sensor. (3) Water tank. (4) Traverse frame. (5) Thermocouples. (6) Test piece. (7) A25 crucible with filled molten aluminium

are controlled by the adjoint solver, and the displacement per iteration is adjusted based on the step size of the steepest descent method [32]. The steepest descent algorithm is a simple form of gradient method requiring information from the objective function and its gradient [32], which in one dimension can be represented as

$$\begin{aligned} x_{k+1} &= x_k - \alpha_k d_k \\ d_k &= J'(x_k) \end{aligned} \quad (10)$$

The step sizes α_k of each objective parameter are selected by trial and error to give a consistent deformation per iteration relative to the baseline geometry. The step size for

surface temperature standard deviation (STSD) was found to be $1\text{E-}8$, which generates 0.26% displacement. The step size for the pressure drop (PD) was found to be $1.5\text{E-}6$, which generates 0.5% displacement. The computed cumulative morph displacement of an arbitrary node of the mesh combines the results of both parameter arrays.

A loop operation is created for the iterative surface optimisation with stopping criteria and loop count specified to monitor the maximum skewness and face validity [45]. To minimise errors generated by deformed cells, the mould and coolant channel are re-meshed if the mesh quality drops below 95%.

2.1.4 Transient model

The transient model is similar to the steady state model, with transient terms added as required to each equation. STARCCM+ is used to solve the solid energy and fluid flow in the cast, mould, and coolant water. An implicit unsteady model is enabled to obtain a more accurate solution for validating the optimised geometry against the experiment dataset. The initial time step Δt is set to 5 ms. The Courant number (CFL) is defined as the ratio of the physical time step Δt to the mesh convection time scale which relates the mesh cell dimension Δx to the mesh flow speed as follows:

$$C = \frac{u\Delta t}{\Delta x} \leq C_{max} \quad (11)$$

Default target mean and maximum CFL numbers are specified as 0.5 and 5, respectively. Adaptive time-stepping is then used to control the CFL number automatically in order to attain the desired temporal resolution and improve simulation stability across widely varying time scales. The volume of fluid (VOF) multiphase model for the molten aluminium is used to analyse the flows of immiscible fluids and to resolve the interface between phases of the mixture. The volume fraction of aluminium i is linked to the volume of the cell V and the volume of the aluminium phase V_i in the cell and can be written as

Table 2 Experimental system components specifications

| Component | Make and model | Key specifications |
|---------------------|--|---|
| Type-K thermocouple | Universal Thermosensors® TC01-10-DKSG-125-YA-2000-L94K-ZCK-IEC | Exposed junction 1 mm diameter, Temperature range – 200 to + 1100 °C, accuracy ± 5 °C |
| Furnace | Nabertherm® K4_10_R7 | Capacity 4L. Crucible type A25, temperature 1200°C |
| Traverse frame | RS PRO® Aluminium Strut | Profile: 40 × 40 mm, Groove size: 8 mm, Material: anodized aluminium |
| Mounting arm | Igus ® Positioning Table SHT-12-AWM-100 mm | Load: 2800 N |
| Logging meter | Omega® OM-DAQXL 8 Channel data logger | Range: – 200 to 1820 °C, Accuracy: $\pm 0.15\%$ reading |
| Water pump | Pentair® Shurflo Aqua King II Model 4158–153-E75 | 12 V DC 5.0GPM [18.9 LPM] 55PSI [3.8BAR] |
| Flow rate sensors | TurboFlow® FT-110 M Series | Accuracy $\pm 3\%$ reading Flow rate: 2–25 L/min Brass design |

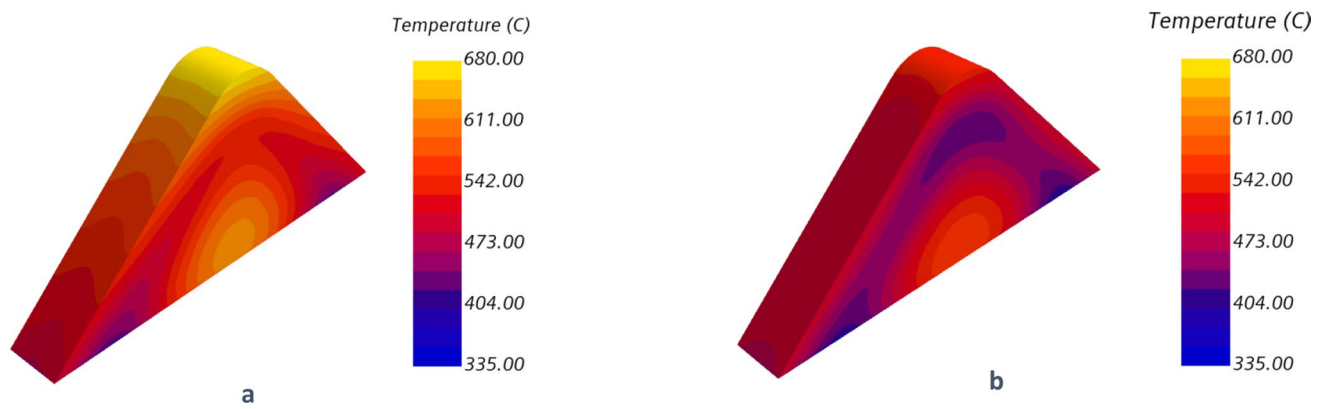


Fig. 10 Temperature distribution on the mould interface side for **a** baseline and **b** optimized corner cooling channel

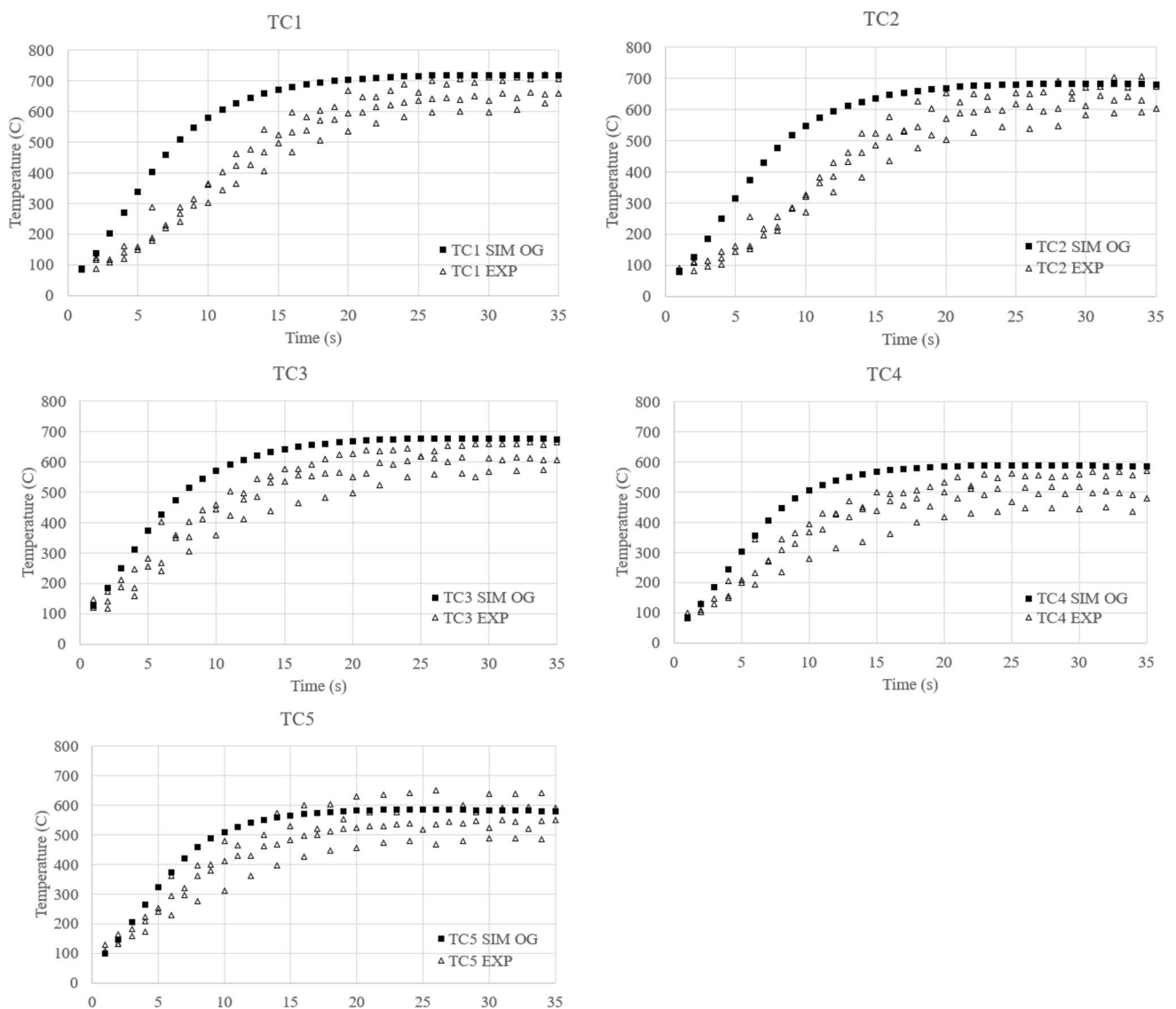


Fig. 9 Temperature variation of the baseline corner cooling design between simulation and experimental solutions

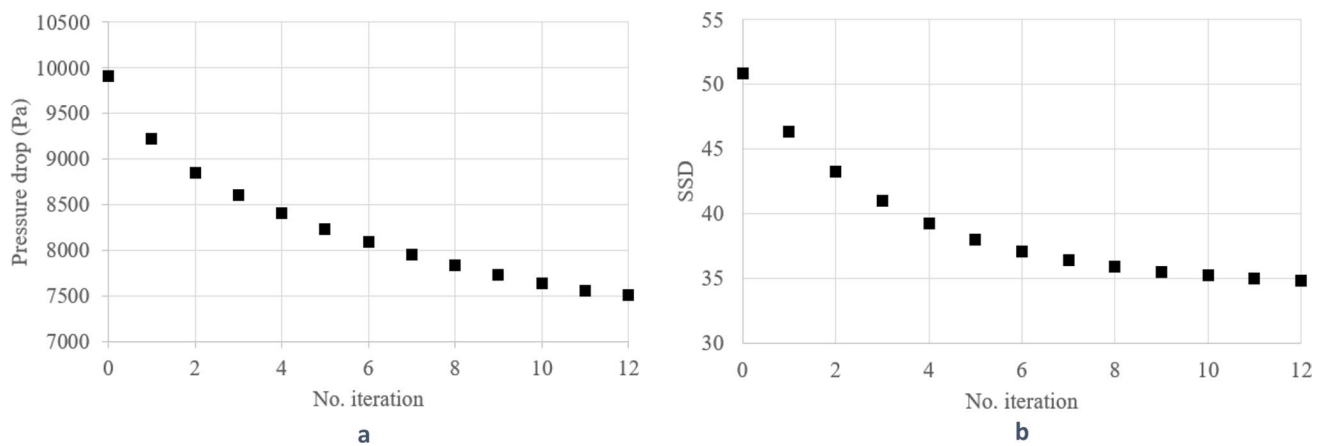


Fig. 11 Convergence study of **a** pressure drop and **b** surface temperature standard deviation against number of iterations

$$\alpha_i = \frac{V_i}{V} \quad (12)$$

The volume fractions of all phases in each cell are satisfied by the following relation:

$$\sum_{i=1}^N \alpha_i = 1 \quad (13)$$

The total number of phases $N = 2$ represents the aluminium in solid and liquid. The presence of different phases or fluids in a cell is categorised using:

$$\begin{cases} \alpha_i = 0, \text{ the cell is completely void of phase } i \\ \alpha_i = 1, \text{ the cell is completely filled with phase } i \\ 0 < \alpha_i < 1, \text{ presence of an interface between phases} \end{cases}$$

An initial volume fraction of 1 is defined for the molten aluminium. The use of the multiphase model enables the melting-solidification flow solver embedded in STAR-CCM+ to simulate the solidification process of molten aluminium. An enthalpy formulation to determine the distribution of the solidified portion of the liquid–solid phase is adapted with the enthalpy of the liquid–solid phase h_{1s}^* written as

$$h_{1s}^* = h_{1s} + (1 - a_s^*)h_{fusion} \quad (14)$$

where h_{1s} represents the sensible enthalpy and h_{fusion} represents the latent heat of fusion. The relative solid volume fraction a_s^* represents the portion of the solidified phase, which is a function of the temperature assuming linear dependency:

$$a_s^* = \begin{cases} 1 & \text{if } T^* < 0 \\ 1 - T^* & \text{if } 0 < T^* < 1 \\ 0 & \text{if } 1 < T^* \end{cases}$$

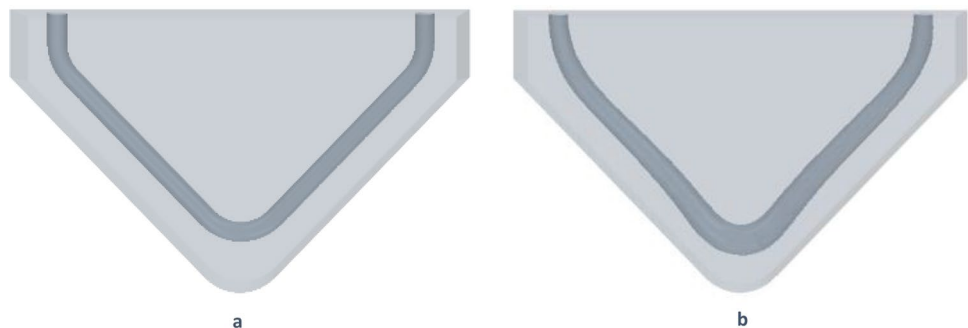
Normalised temperature T^* can be defined as

$$T^* = \frac{T - T_{solidus}}{T_{liquidus} - T_{solidus}} \quad (15)$$

The initial state of the AlSi9 aluminium casting alloy is set to liquid with a temperature of 750 °C. Additional material properties such as liquidus and solidus temperature are provided in Table 1.

It is necessary to consider the cooling channel surface roughness in this transient validation model since all inserts with the conformal cooling layouts were manufactured via a DMLS machine. Based on the evaluation of the industrial test piece of average roughness Ra and peak-valley difference Rz, a 0.3 mm wall surface

Fig. 12 **a** Baseline surface and **b** optimized surface design of the corner cooling channel



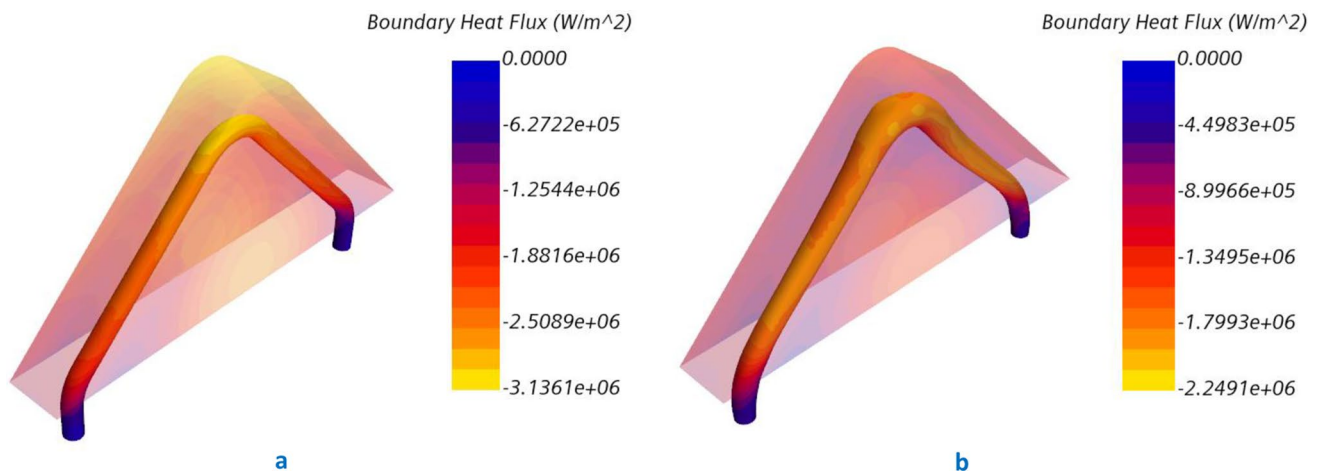


Fig. 13 Boundary heat flux distribution on **a** baseline and **b** optimised cooling channel surface

roughness was specified around the inner cooling channels. As described above, the IHTC at the mould/cast interface falls rapidly once the aluminium is in contact with the mould surface, settling to an almost steady value between 3500 and 7000 W/m² K within a few seconds. Here, we model the HTC from the interfacial resistance based on the surface roughness of the mould, cast, or coating layer [31, 42]. A constant IHTC of 5000 W/m² K is defined between the aluminium cast with non-coated mould steel for our initial transient model. The initial variation of HTC, however, still depends on the experimental setup and placement of the thermocouples. This will be critical when calibrating the numerical and experimental data in the results section.

2.2 Furnace design + experimental setup

The baseline of the corner cooling test piece was designed and 3D-printed to allow full submersion inside the aluminium-filled standard A25 crucible. The level of submersion matches the bottom line of the side square surfaces as demonstrated in Fig. 5. The design piece was manufactured via a DMLS machine with a surface finish around all exposed surfaces. Extensions of five times the length of the pipe diameter are implemented at the channel inlet and outlet to ensure fully developed flow before the bend.

Special attention has been paid to the placement of thermocouples and the type of thermocouple insulation to achieve a reasonable response time and precision of the reading [35]. A 1 mm diameter mineral insulated exposed junction type-K thermocouple was chosen for all our measurements. Eight thermocouples are used for the corner design case as shown in Fig. 6. TC1–5 are located 2 mm away from the bottom surface with 20 mm separation. TC 6–8 are calibration points located at the inlet, outlet, and highest temperature zone of the corner design, respectively. Thermocouple readings are recorded at 200 ms intervals.

The experimental setup for the corner design piece and a generalised diagram for the furnace test rig are shown in Figs. 7 and 8, respectively, with specifications of the main components tabulated in Table 2. The furnace consists of three main sections. The top lid can be opened allowing test pieces to be inserted or removed. The middle section consists of the A25 crucible surrounded by foam to reduce heat loss. The furnace stand, electrical supply, switches, and monitor screen are in the lower section. The furnace has an internal control system to maintain the aluminium temperature at a constant value. The test piece is mounted on a 2-D manual traverse wheel-guided mechanism that adjusts the horizontal and vertical position of the test piece to line it up with the centre of the crucible at the appropriate immersion depth. The coolant inlet/outlet channels are connected via a storage tank and water circuit. The tank water temperature is maintained at 70 °C (±5 °C). The cooling water flow rate is kept constant at 7 L/min (±0.2 L/min). Measurements from the temperature and flow control systems are recorded by the data acquisition system.

3 Results

Results are presented in three parts. Firstly, the transient simulation solution for the baseline corner cooling design is compared with experimental data to demonstrate that the thermal model is valid for the next optimisation stage. Secondly, optimisation results for the adjoint method are presented for the corner baseline design. These include convergence analysis, discussion of the optimised internal cooling design, and thermal analysis of the temperature distribution across the mould/cast interface between the baselines and optimised cooling layout. Finally, the adjoint method CFD results are compared with experimental data. This reveals significant disagreements which are resolved

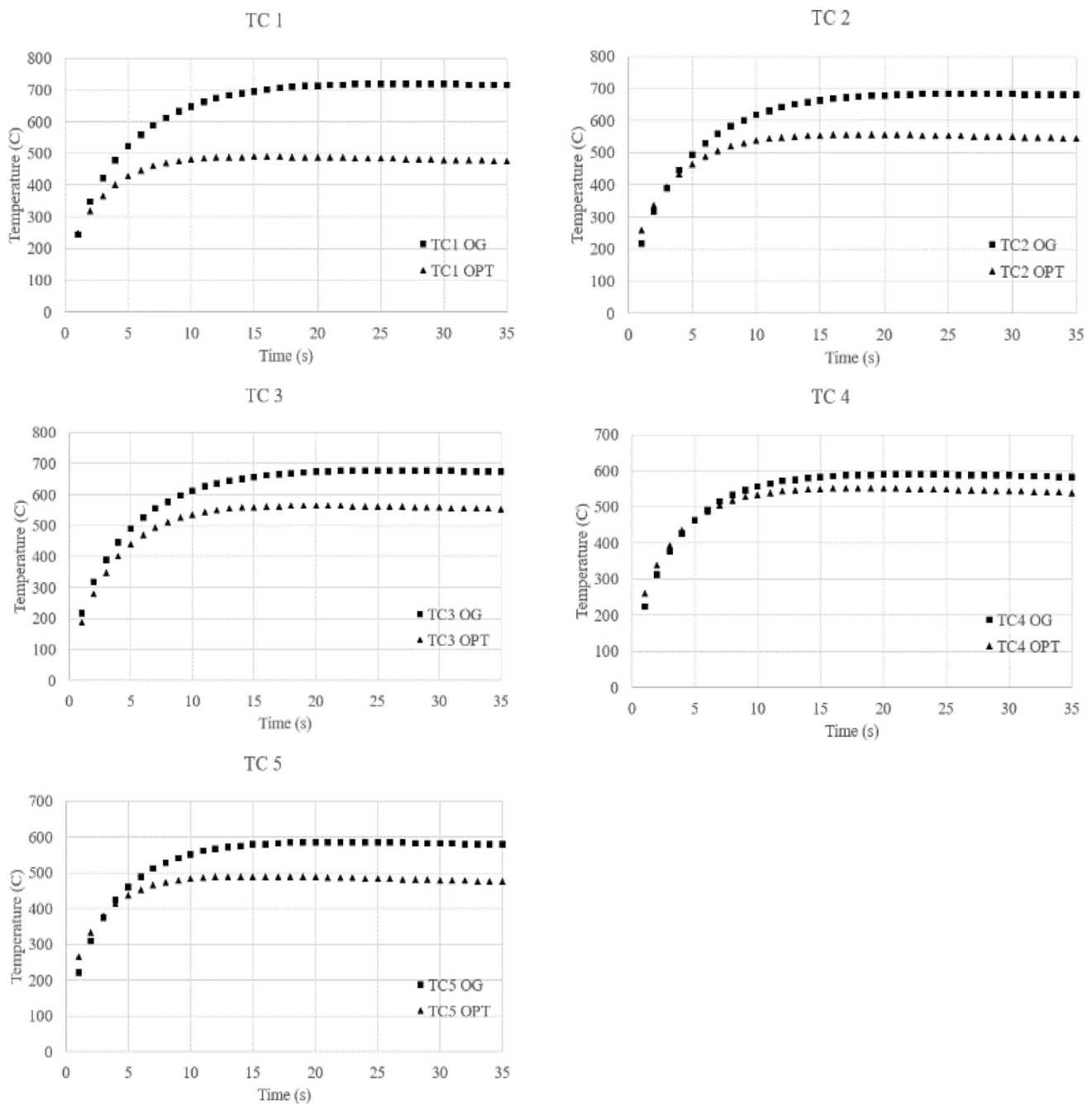


Fig. 14 Thermal model temperature variation between baseline and optimized corner cooling design of the centre five thermocouple locations

by the introduction of a new IHTC model to calibrate the transient model. A discussion of error sources is included.

3.1 Initial baseline thermal transient model validation

The initial thermal model for the baseline corner cooling design is validated via a series of experiments. The recording period is set to 35 s to adequately record the key stages of

the solidification process. Figure 9 compares experimental results from thermocouples TC1-5 with the corresponding simulation results for five repeated trials. All locations show a rapid rise in temperature from an initial value of around 100 °C to between 500 and 700 °C, which is maintained to the end of the 35 s period. There is clear disagreement in the rate of change of temperature increase between experimental and simulated data. However, all simulation peak temperatures fall within the range of the various experimental trials.

Table 3 Thermocouple monitor points results

| | Max T °C Original | Max T °C Optimised | ΔT °C | % Drop |
|----------------------|----------------------|-----------------------|---------------|--------|
| Simulation results | | | | |
| TC1 | 719.0 | 489.1 | 229.9 | 32.0 |
| TC2 | 683.0 | 555.6 | 127.4 | 18.7 |
| TC3 | 677.8 | 563.7 | 114.1 | 16.8 |
| TC4 | 589.5 | 550.5 | 39.0 | 6.6 |
| TC5 | 585.4 | 489.6 | 95.8 | 16.4 |
| Experimental results | | | | |
| TC1 | 694.9 | 444.5 | 250.3 | 36.0 |
| TC2 | 668.0 | 537.9 | 130.1 | 19.5 |
| TC3 | 642.2 | 587.1 | 55.1 | 8.6 |
| TC4 | 536.6 | 506.4 | 30.2 | 5.6 |
| TC5 | 584.9 | 426.7 | 158.1 | 27.0 |

The adjoint optimisation must be conducted under steady-state conditions, and as discussed in the introduction, the initial liquid aluminium temperature is raised to 750 °C to ensure a prolonged steady state period before the molten cast is fully solidified. Both the initial steady simulation and the baseline experiments capture this asymptotic period before solidification.

Accordingly, it is considered that there is sufficient agreement between the simulated and experimental results to proceed with the subsequent optimisation work. The discrepancy during temperature rise is less of a concern for the steady model; however, it is addressed again in the final transient model calibration as described in Sect. 3.3.2.

3.2 Steady model obtaining primal solution and adjoint optimisation results

Ensuring convergence for the primal solution is critical, especially as all subsequent analyses will be based on the initial baseline result. A total of 8000 iterations are performed, resulting in all conservation equation residuals dropping below $1E-5$. Variations in the cost function parameters PD and STSD are monitored in order to detect convergence. When the variation in both values drops below 0.1% over 10 iterations, it is assumed that steady state has been reached, with the simulation continuing until the residual limit is achieved. The PD and STSD values are found to be 9912.2 Pa and 50.86 °C, respectively. The thermal distribution at the mould/cast interface for the initial baseline cooling design is shown in Fig. 10a. A hot temperature zone occurs at the corner region with a maximum temperature of 678.72 °C. The high temperature around the internal corner

surface is attributed to the limited area available to dissipate the heat to the cooling channels [13, 27]. Low-temperature areas are located on the external side of the corner surface with a minimum value of 359.93 °C.

Figure 10b shows the thermal distribution along with the mould/cast interface for the optimised corner cooling channel. The high-temperature zone at the corner is significantly refined compared to the baseline design in Fig. 9a. Low-temperature regions remain at the approximate same area around the inlet/outlet cooling channel.

Figure 11 shows the variation in the PD and STSD over 12 optimisation iterations. In each iteration, the channel surface is deformed to reduce the objective function as explained in Sect. 2.1.2. The final geometry of the cooling channels delivers a PD reduction of 24.2% to 7509 Pa and an STSD reduction of 31.6% to 34.81 °C. The maximum temperature drop of the sidewalls is also reduced from 678.72 to 569.32 °C (16.1%).

Figure 12 shows the internal pipe surface for both baseline and optimised cooling design after twelve iterations of deformation. An increase in pipe diameter across all segments of the corner design was generated in the optimal design, with the largest increase in the corner region. A slight deviation of the cooling pipe away from the surface can be observed just before the bend region. Additional refinement/smoothing of the cooling pipe geometry can also be seen around the coolant inlet and outlet regions.

The adjustments in pipe geometry are reflected in the boundary heat flux along the cooling channel surface shown in Fig. 13. The baseline design shows a high boundary heat flux in a small corner area compared with the rest of the cooling surfaces. This indicates a significant amount of heat being dissipated at this location, resulting in a high local temperature and a large temperature gradient to the remaining cooling surfaces. Conversely, the optimised corner cooling channel has a more uniform dissipating boundary heat flux value. This leads to a more consistent cooling rate at the corner pipe surfaces and thermal uniformity along with the mould/cast contact interface.

The IHTC between the aluminium cast and mould steel is an important factor in determining the true interface temperature. However, in this first design, minimising the temperature variation is the aim rather than predicting the absolute value. By assuming the thermal resistance is the same across the entire interface, the effect of HTC change can be considered negligible, unless there is a large variation in cast thickness [40]. Variation in HTC is however considered in the next section where a transient thermal model is developed and validated against the experimental results.

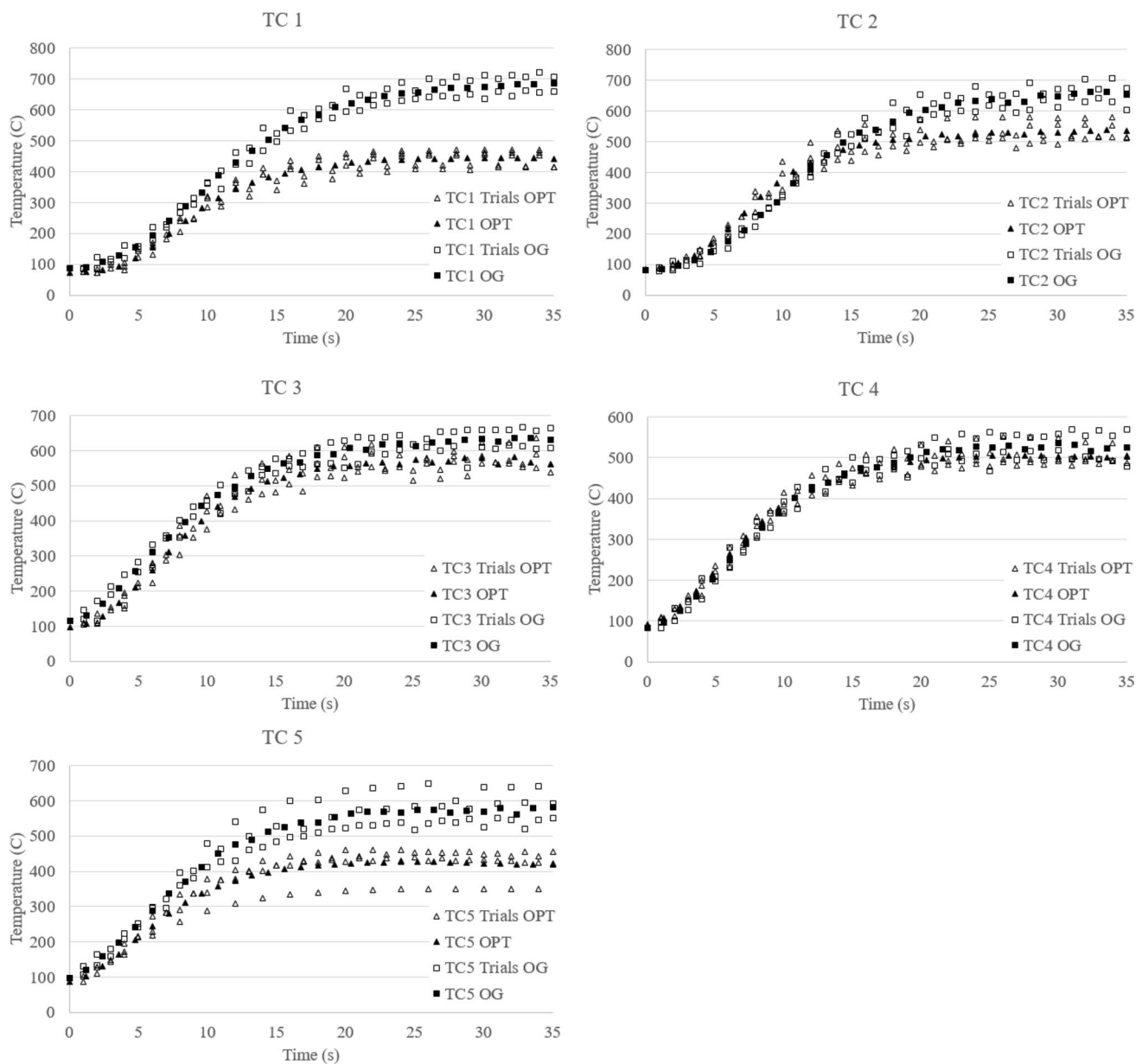


Fig. 15 Experimental temperature variation between baseline and optimized corner cooling design of the centre five thermocouple locations

3.3 Comparison between the thermal model and experiment results

3.3.1 Comparison between the baseline and the optimised geometries results

Simulated TC1-5 temperature variations for the baseline and optimised geometries are plotted in Fig. 14. All locations show an increase reaching an almost constant value after approximately 15 s. Peak temperatures are listed in Table 3 together with the peak temperature reduction for the optimised case, in both relative and absolute values which, for TC1, is 230 °C and 32%, respectively.

Experiments are conducted using manufactured versions of the baseline and optimised corner cooling mould configurations, with four repeat trials per design. The results for each trial are shown in Fig. 15 together with an average trend for each design, with peak values shown in Table 3. In these experimental results, TC1 and TC5 show peak temperature drops of 250 °C (36%) and 158 °C (27%), respectively. Overall, the significant reduction in peak temperature observed experimentally demonstrates the improved performance of the optimised design.

By comparing the solution between the simulation and experimental trials in Fig. 14, all thermocouples reach asymptotic steady temperature values, showing good agreement with the

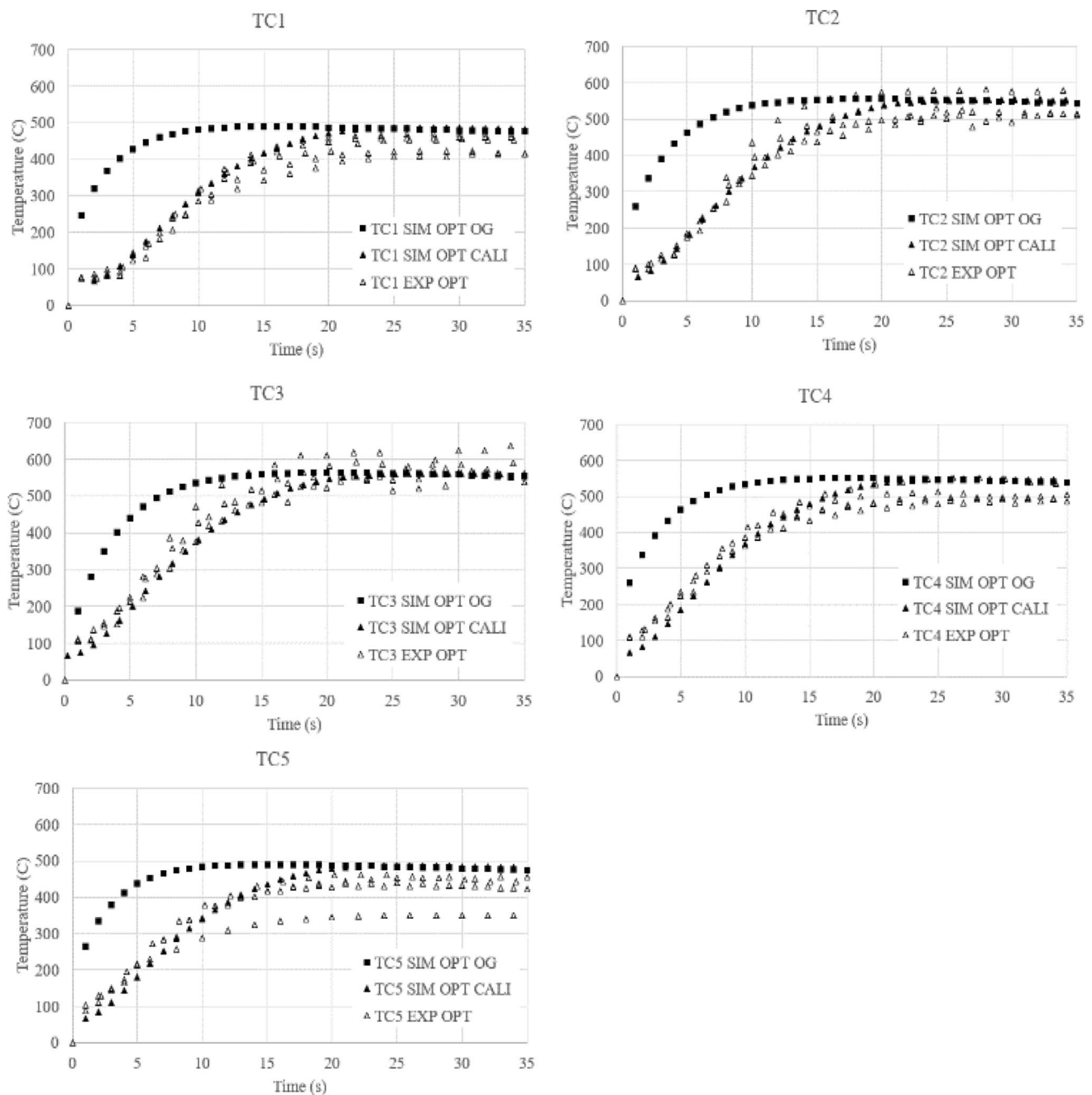


Fig. 16 Calibration of temperature variation between baseline and optimized corner cooling design of the centre five thermocouple locations

simulation results. Although there are small differences in the max temperature at each location, the temperature gradients are almost identical in both absolute values and percentages.

3.3.2 Thermal model calibration during the transient period

Although the simulated and experimental asymptotic temperature values show good agreement, there is significant variation in the temperature and duration of the initial

transients, as shown in Fig. 14. Discrepancies occur at all locations, suggesting a common factor. We suggest this is the complex physics of the solidification process and its influence on the interface heat transfer coefficient. Assuming the experimental results are accurate enough, then the model needs to be calibrated if simulation and experiment are to be reconciled.

As discussed above, the IHTC has significant variation throughout the casting. Here, we apply a bounded linear model as follows:

Fig. 17 Industrial HPADC mould design and layout of the **a** aluminium cast (green), **b** conventional and conformal cooling channel locations (purple)

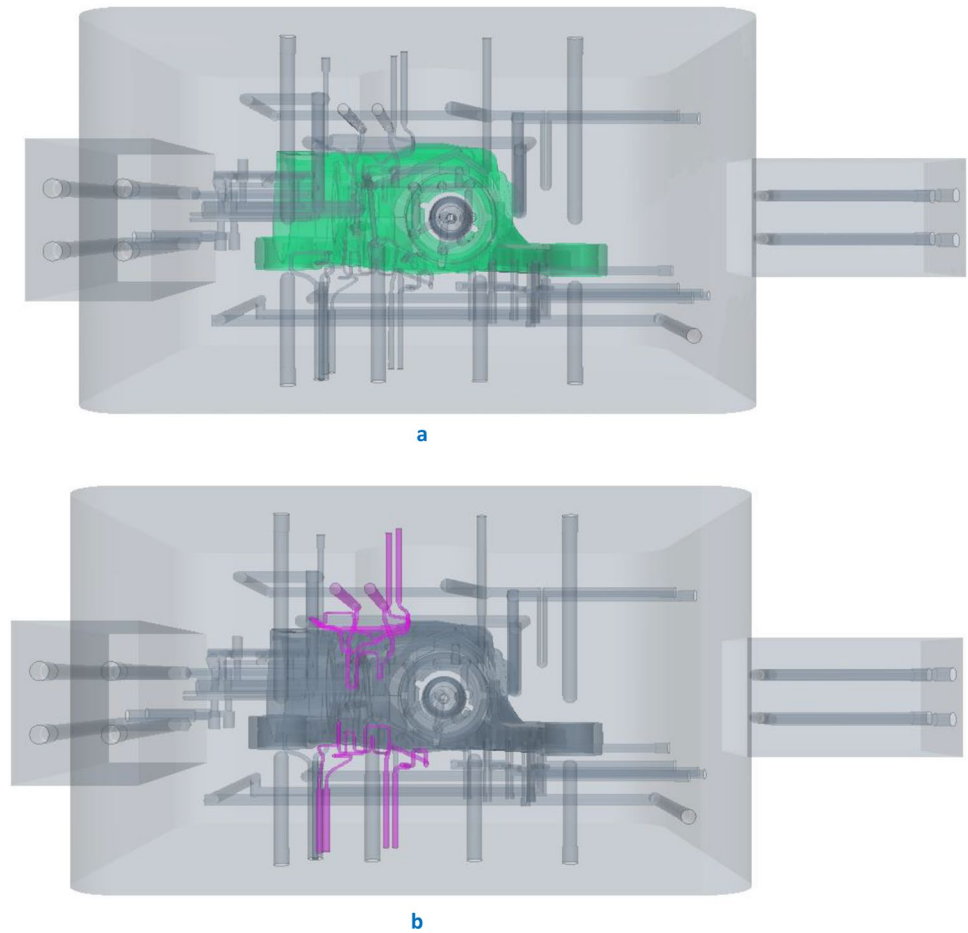
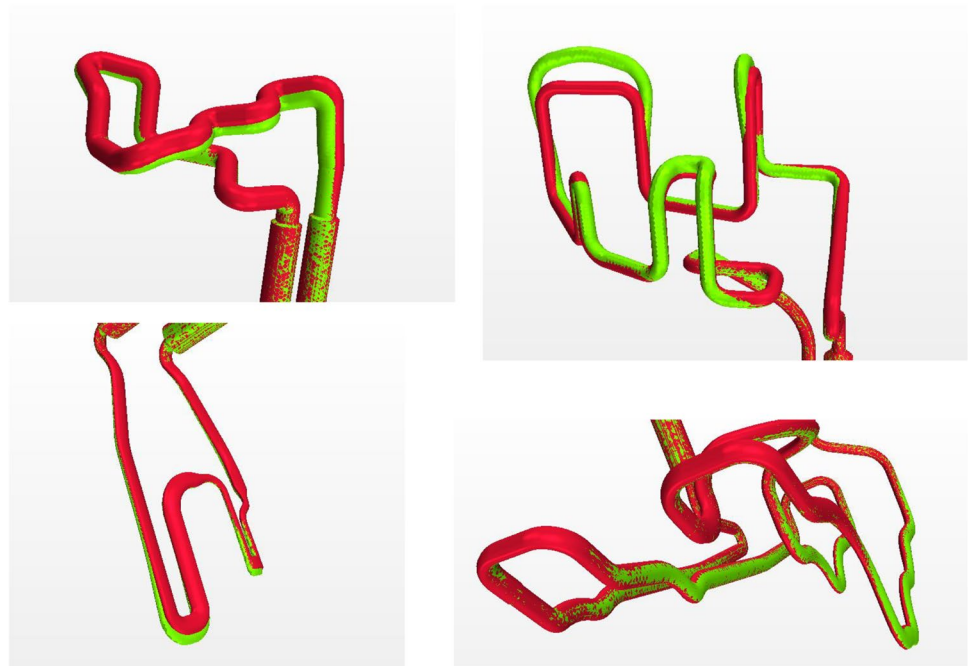


Fig. 18 Comparison between baseline (red) and optimised (green) cooling profile of the four conformal cooling pipes for the industrial mould



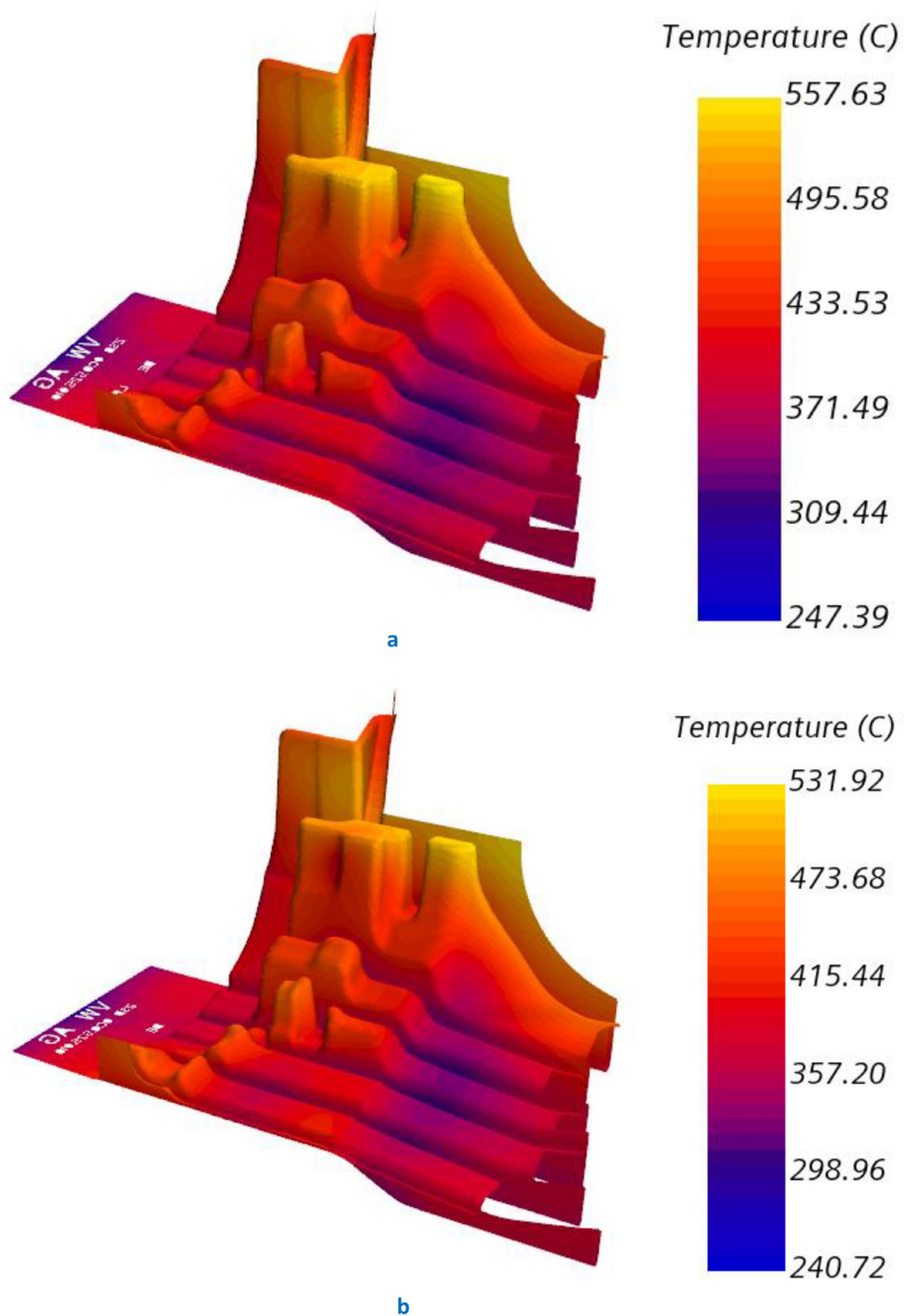
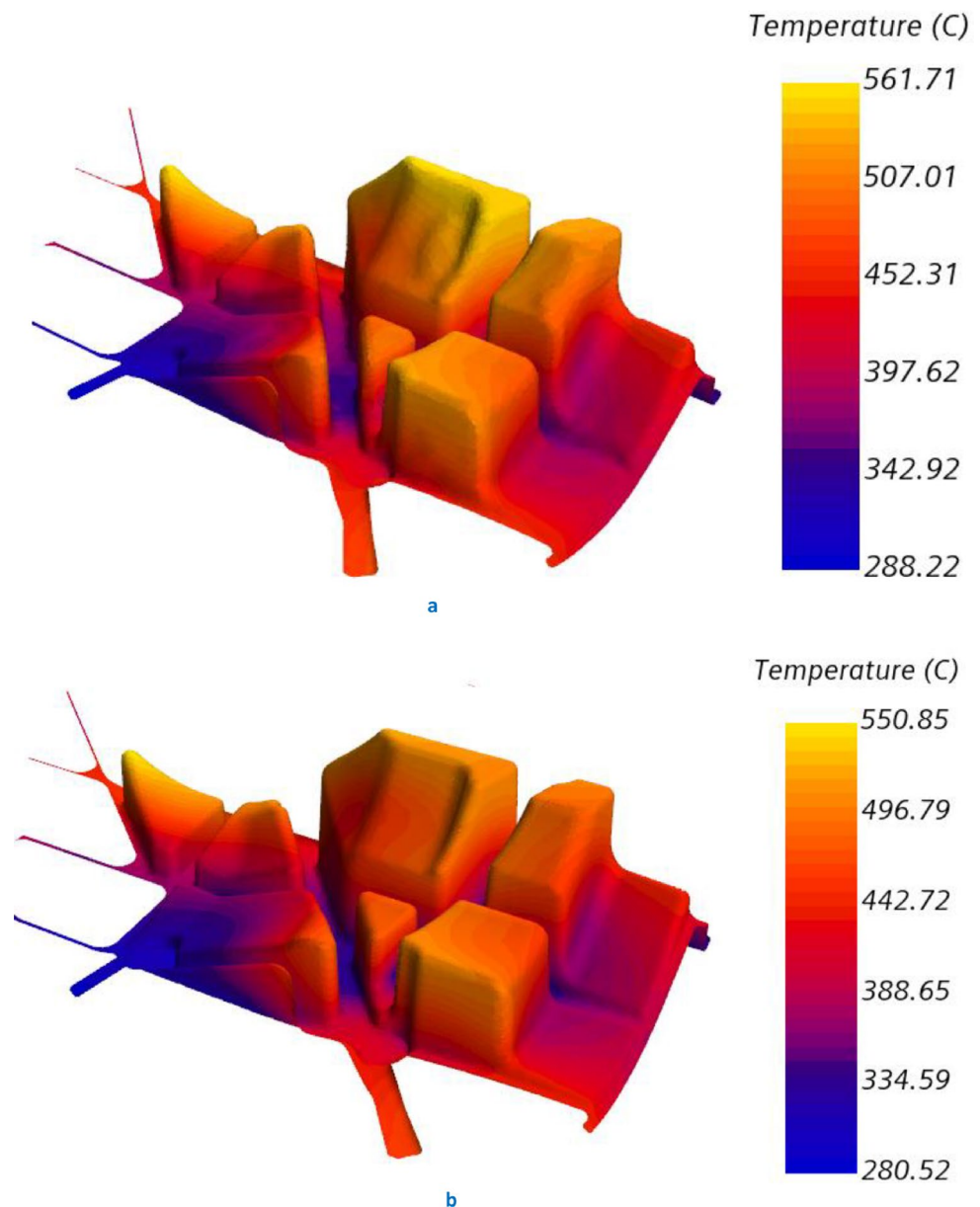


Fig. 19 Temperature distribution across mould/cast interface for both **a** baseline and **b** optimal oil-cooling channel designs

Fig. 20 Temperature distribution across mould/cast interface on both **a** baseline and **b** optimal water-cooling channel designs



$$h(t) = \begin{cases} 250t, & 0 < t \leq 20(s) \\ 5000, & t > 20(s) \end{cases}$$

Applying this model to the simulation, much better agreement with the experimental results is obtained, as shown in

Table 4 Surface temperature and average boundary heat flux results

| | Oil side | Water side | Overall |
|--|----------|------------|---------|
| Temperature surface standard deviation | | | |
| Original cooling design | 61.8 | 61.2 | 65.9 |
| Optimised cooling design | 56.2 | 56.0 | 56.0 |
| Average boundary heat flux (W/m ²) | | | |
| Original cooling design | 3.05E5 | 4.98E5 | 3.76E5 |
| Optimised cooling design | 2.84E5 | 4.73E5 | 3.54E5 |

Fig. 16, with all calibrated simulation results falling within the scattered experimental data range. A more complex model can be investigated by considering the topography of the mould-cast contact surfaces and analysing the surface roughness and trapped air gap using the Hamasaiid concept [43].

4 Implementation in industrial HPADC tool

The adjoint optimisation technique has been applied to the design of the cooling system of an industrial high-pressure aluminium die-casting (HPADC) tool. The Buhler-Prince HPADC machine manufactures gearbox housing components [40]. This has two main steel bodies fitted with both

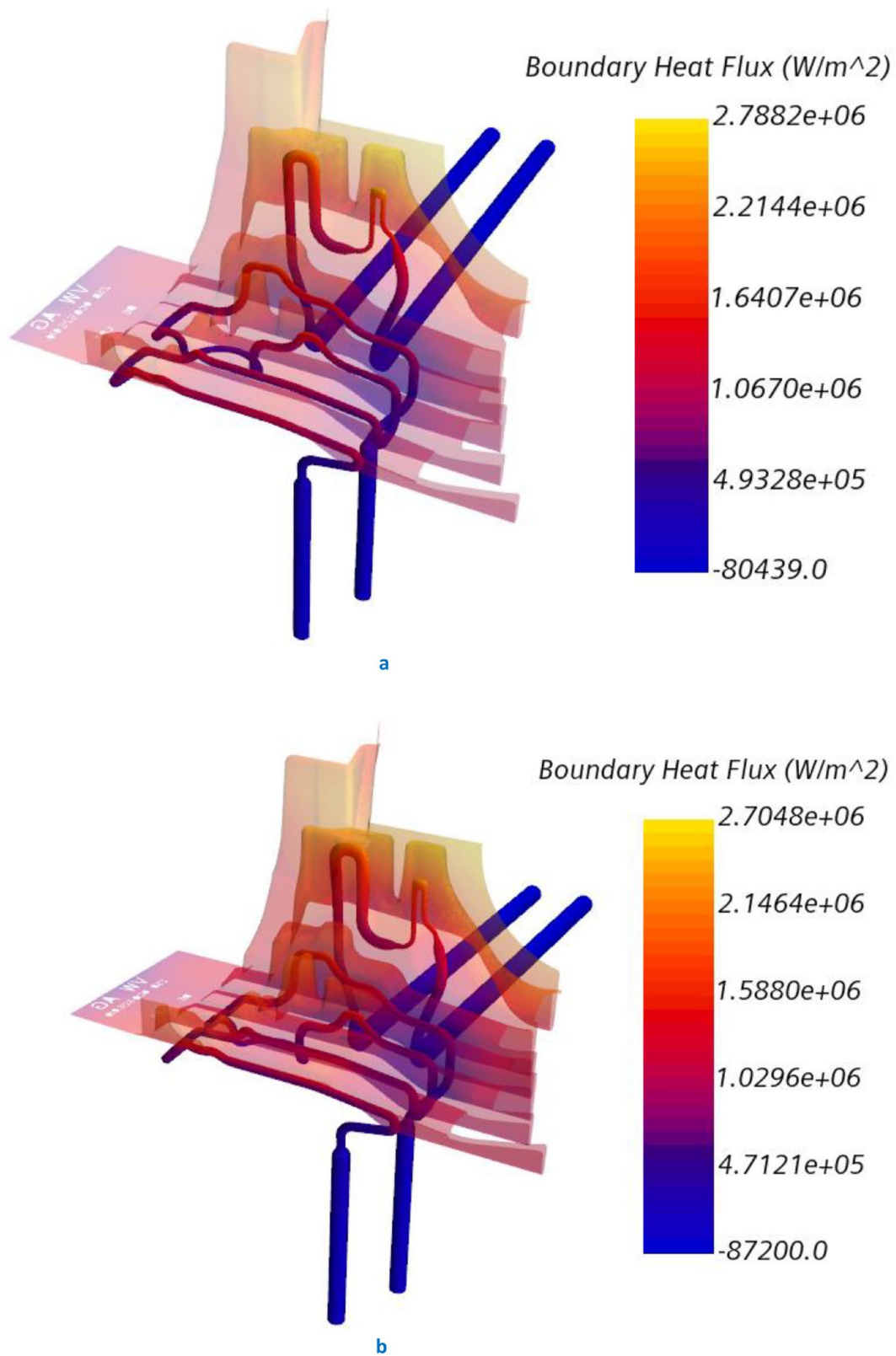


Fig. 21 Boundary heat flux distribution across mould/cast interface for both **a** baseline and **b** optimal oil-cooling channel designs

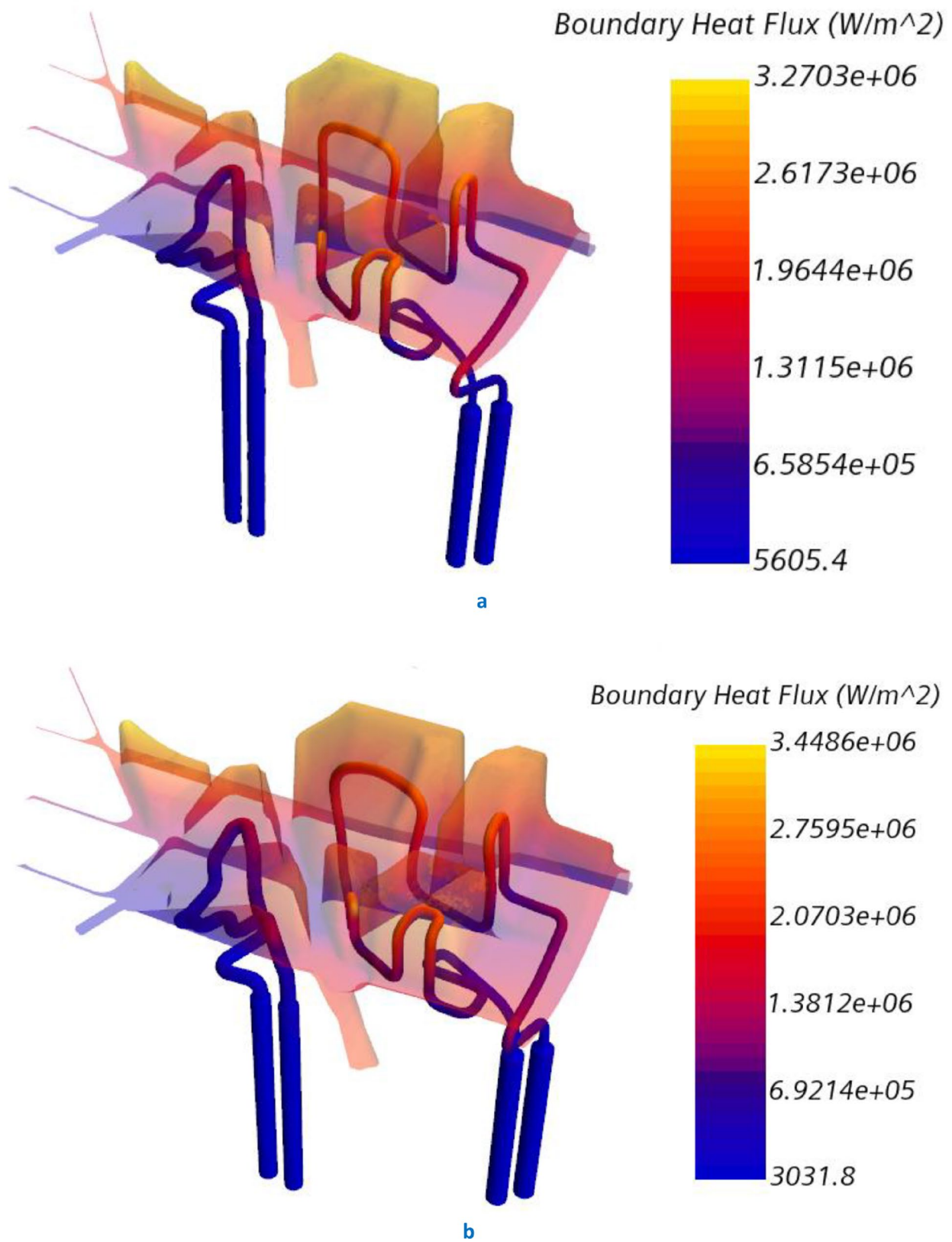


Fig. 22 Boundary heat flux distribution across mould/cast interface for both **a** baseline and **b** optimal water-cooling channel designs

conventional cooling channels and removable conformal cooling inserts as shown in Fig. 17, which also highlights the complex casting shape. The optimisation technique has been used to refine the four sets of 6 mm conformal cooling inserts, two using oil and two using water, all operating at 3 L/min. In this application, design optimisation aims to reduce the thermal gradient at the contact interface in order to prolong tooling life. The effects of the pressurised condition in the aluminium die-casting process in affecting the IHTC have been addressed in the “Introduction” section. Since its duration takes up a small percentage of the whole casting period, the initial forced injection condition has been neglected, and a constant IHTC of $5000 \text{ W/m}^2 \text{ K}$ is assumed. The remaining simulation model setup for the complex geometry follows the same procedures as the baseline study described above.

Optimised profiles compared to the baseline design of both oil and water-cooling channel sets are presented in Fig. 18. Results with their associated cooling surfaces are presented separately in Figs. 19 and 20. The temperature gradient along the oil-cooled surface shows a decrease from baseline 310.24 to 291.2 °C, and for the water-cooling side from 273.49 to 270.33 °C. These reductions may seem less significant; however, the mould/cast interface temperature standard deviation tabulated in Table 4 shows a more uniform cooling has been achieved by 8.99% for oil-cooling and 8.52% for water-cooling of the optimised conformal pipe inserts. Overall, a 15% reduction in temperature variation has been achieved for the entire mould/cast contact surface.

The enhanced uniform cooling effect can also be explained by the more consistent boundary heat flux around the optimised cooling pipe surfaces as shown in Figs. 21 and 22. The maximum boundary heat flux on the baseline corner surface shows much greater values than any of the optimised oil or water pipe surface, which end up with a high local temperature and large gradient to the surrounding surfaces.

The optimised cooling system design delivers a lower thermal gradient at the contact interface by morphing the pipe surface to obtain a lower and more consistent heat-dissipating boundary heat flux value at the pipe surfaces, achieving (Table 4) an overall 5.85% reduction for all four conformal cooling inserts. Applied as an industrial manufacturing system, the optimised four conformal inserts working together with the conventional cooling system of the HPADC tool increased operational lifespan from 40,000 to 120,000 cast cycles.

5 Summary/conclusions

This study has described the application of the adjoint method to optimise a baseline corner conformal cooling design for an aluminium gravity die-casting system via the commercial CFD software STARCCM+. The aim has

been to achieve better uniform cooling between the mould and cast interface during the solidification process while maintaining a lower pressure drop within the pipe, thereby enhancing the thermal performance of the entire process and achieving prolonged tooling life for the casting tool. An experimental setup was developed to validate the model. The optimised corner design features a cooling channel cross section which gradually widens towards the corner and in simulation results in a 31.6% reduction in temperature standard deviation across the contact interface (i.e. achieves more uniform cooling) and a 24.2% reduction in pressure drop across the whole cooling channel. After 3-D printing and experimentally testing the baseline and the optimised geometries, good agreement was achieved once an IHTC model was introduced to account for varying the thermal resistance between the cast and mould. The improvements moving from the baseline to optimised designs were significant, with a temperature drop of 36% observed at one location. The adjoint optimisation technique has been applied to the design of the cooling system of a complex industrial HPADC tool, with the aim of improving the uniformity of the interfacial cooling. The resulting design has delivered an increase in the operation life of the tool from 40,000 shots to almost 120,000 shots. In summary, this study has developed an optimisation model using the adjoint method with multi-objective functions. This simplified algorithm was applied to the HPADC process and resulted in extended tooling life. Our future work aims at implementing the adjoint topology method for the initial layout of the conformal cooling pipes.

Acknowledgements The author would like to acknowledge CastAlum Team for their contribution and the technical support. The authors would like also to acknowledge Innovate UK project no P16874 and Engineering and Physical Sciences Research Council EPSRC Reference EP/V02695X/1 for the fund.

Author contribution All authors contributed to study conception and design. The first draft of the manuscript was written by Tongyan Zeng, and all authors commented on the previous version of the manuscript. All authors read and approved the final manuscript.

Declarations

Conflict of interest The authors declare no competing interests.

Open Access This article is licensed under a Creative Commons Attribution 4.0 International License, which permits use, sharing, adaptation, distribution and reproduction in any medium or format, as long as you give appropriate credit to the original author(s) and the source, provide a link to the Creative Commons licence, and indicate if changes were made. The images or other third party material in this article are included in the article's Creative Commons licence, unless indicated otherwise in a credit line to the material. If material is not included in the article's Creative Commons licence and your intended use is not permitted by statutory regulation or exceeds the permitted use, you will need to obtain permission directly from the copyright holder. To view a copy of this licence, visit <http://creativecommons.org/licenses/by/4.0/>.

References

- Othmer C (2008) A continuous adjoint formulation for the computation of topological and surface sensitivities of ducted flows. *Int J Numer Meth Fluids* 58:861–877
- Kitayama S, Miyakawa H, Takano M, Aiba S (2017) Multi-objective optimization of injection molding process parameters for short cycle time and warpage reduction using conformal cooling channel. *Int J Adv Manuf Technol* 88:1735–1744
- Singraur DS, Patil B (2016) Review on performance enhancement of plastic injection molding using conformal cooling channels. *Int J Eng Res General Sci* 4(4)
- Sachs E et al (2000) Production of injection moulding with conformal cooling channels using the three-dimensional printing process. *Polym Eng Sci* 40(5):1232–1247
- Hassan H, Regnier N, Pujos C, Arquis E, Defaye G (2010) Modeling the effect of cooling system on the shrinkage and temperature of the polymer by injection molding. *Appl Therm Eng* 30(13):1547–1557
- Sanchez R, Aisa J, Martinez A, Mercado D (2012) On the relationship between cooling setup and warpage in injection moulding. *Measurement* 45(5):1051–1056
- Tong W et al (2017) Design optimisation of plastic injection tooling for additive manufacturing. *Procedia Manuf* 10:923–934
- Kuo C-C (2017) A new method of manufacturing a rapid tooling with different cross-sectional cooling channels. *Int J Manuf Technol* 92(9–12):3481–3487
- Ahn DG, Kim HW (2010) Study on the manufacture of a thermal management mould with three different materials using a direct metal tooling rapid tooling process. *Proc Inst Mech Eng B J Eng Manuf* 224(3):385–402
- Saifullah ABM et al (2012) Thermal-structural analysis of bi-metallic conformal cooling for injection moulds. *Int J Manuf Technol* 62:123–133
- Altat K et al (2016) Determining the effects of thermal conductivity on epoxy moulds using profiled cooling channels with metal inserts. *J Mech Sci Technol* 30(11):4901–4907
- Ferreira JC, Mateus A (2003) Studies of rapid soft tooling with conformal cooling channels for plastic injection moulding. *J Mater Process Technol* 142:508–516
- Kanbur BB, Suping S, Duan F (2020) Design and optimisation of conformal cooling channels for injection moulding: a review. *Int J Adv Manuf Technol* 106:3253–3271
- Altat K et al (2013) Prototype production and experimental analysis for circular and profiled conformal cooling channels in aluminium filled epoxy injection mould tools. *Rapid Prototyp J* 19(4):220–229
- Rahim SZA et al (2016) Improving the quality and productivity of moulded parts with a new design of conformal cooling channels for the injection moulding process. *Adv Polym Technol* 35(1):21524
- Brooks HL (2016) Design of conformal cooling layers with self-supporting lattices for additively manufactured tooling. *Addit Manuf* 11:16–22
- Lions JL (1971) Optimal control of systems governed by partial differential equations (Grundlehren der Mathematischen Wissenschaften), vol 170. Springer, Berlin
- Pironneau O (1974) On optimum design in fluid mechanics. *J Fluid Mech* 64(1):97–110
- Jameson A (1988) Aerodynamics design via control theory. *J Sci Comput* 3:233–260
- Jameson A (1995) Optimum aerodynamic design using CFD and control theory. In: 12th computational fluid dynamics conference, pp 1729
- Baysal O, Eleshaky ME (1992) Aerodynamic design optimisation using sensitivity analysis and computational fluid dynamics. *AIAA J* 30(3):718–729
- Nielsen E, Anderson WK (1999) Aerodynamic design optimisation on unstructured meshes using the Navier-Stokes equations. *AIAA J* 37(11):957–964
- Li Z et al (2018) Topology optimisation for the design of conformal cooling systems in thin-wall injection molding based on BEM. *Int J Adv Manuf Technol* 94:1041–1059
- Xu S, Jahn W, Müller JD (2014) CAD-based shape optimisation with CFD using a discrete adjoint. *Int J Numer Meth Fluids* 74(3):153–168
- Wu T, Tovar A (2018) Design for additive manufacturing of conformal cooling channels using thermal-fluid topology optimization and application in injection molds. In: ASME 2018 International Design Engineering Technical Conferences and Computers and Information in Engineering Conference (pp. V02BT03A007-V02BT03A007). Am Soc Mech Eng. <https://doi.org/10.1115/DETC2018-85511>
- Clark LD, Davey K, Hinduja S (2001) Novel cooling channel shapes in pressure die casting. *Int J Numer Meth Eng* 50:2411–2440
- Abo-Serie E, Jewkes J, Zeng T, Liang Y (2021) Simplified CFD model for assessing the cooling channel design in 3D printed high-pressure tools for aluminium alloy casting. *SAE Technical Papers*, no. 2021, 2021-01-0270. <https://doi.org/10.4271/2021-01-0270>
- Menter FR (1994) Two-equation eddy-viscosity turbulence modeling for engineering applications. *AIAA J* 32(8):1598–1605
- Shehata F, Abd-Elhamid M (2003) Computer aided foundry die-design. *Mater Des* 24:577–583
- Pierce NA, Giles MB (2000) An introduction to the adjoint approach to design. *Flow Turbul Combust* 65(3–4):393–415
- Paul C, Venugopal P (2010) Modelling of interfacial heat transfer coefficient and experimental verification for gravity die casting of aluminium alloys. *International Journal of Mechanical Engineering & Technology (IJMET)* 1(1):253–274
- Hinchliffe BL (2016) Using surface sensitivity for adjoint aerodynamic optimisation of shock control bumps (Doctoral dissertation, University of Sheffield)
- Ho CY, Holt JM, Mindlin H (1992) Structural alloys handbook. Cindas/Purdue University
- Baril E, Labelle P, Pekguleryuz MO (2003) Elevated temperature Mg–Al–Sr: creep resistance. *Mech Prop Microstruct JOM* 55:34–39. <https://doi.org/10.1007/s11837-003-0207-7>
- Long A et al (2011) Determination of the heat transfer coefficient at the metal-die interface for high pressure die cast ALSi-9Cu3Fe. *Appl Therm Eng* 31:3996–4006
- Asthana S (2013) Innovative die lubricant trends for evolving productivity and process requirements. In: Paper T13-062, NADCA 2013 Die Cast Congress
- Graff JL, Kallien LH (1993) The effect of die lubricant spray on the thermal balance of dies. In: Paper T93-083. NADCA Meeting, Cleveland
- Hamasaid A, Dargusch MS, Dour G (2019) The impact of the casting thickness on the interfacial heat transfer and solidification of the casting during permanent mold casting of an A356 alloy. *J Manuf Process* 47:229–237
- Vossel T et al (2021) Heat transfer coefficient determination in a gravity die casting process with local air gap formation and contact pressure using experimental evaluation and numerical simulation. *Int J Metalcast*. <https://doi.org/10.1007/s40962-021-00663-y>
- Griffiths WD, Kawai K (2010) The effect of increased pressure on interfacial heat transfer in the gravity die casting process. *J Mater Sci* 45:2330–2339. <https://doi.org/10.1007/s10853-009-4198-9>
- Anderson JT et al (1997) Experimental investigation and finite element modelling in gravity die casting. *Proc Inst Mech Eng, Part B: J Eng Manuf* 211(2):93–107

42. Hallam CP, Griffiths WD (2004) A model of the interfacial heat-transfer coefficient for the aluminum gravity die-casting process. *Metall Mater Trans B* 35:721–733
43. Hamasaiid Anwar et al (2010) A predictive model for the evolution of the thermal conductance at the casting–die interfaces in high pressure die casting. *Int J Therm Sci* 49(2):365–372
44. Siemens (2021) Siemens digital industries software. Simcenter STAR-CCM+, version 2021.1. <https://www.plm.automation.siemens.com/global/en/products/simcenter/STAR-CCM.html>
45. Siemens. (2021) Siemens industries digital software. Simcenter STAR-CCM+ user guide, version 2021.3. In checking the volume mesh, pages 2794–2837. https://docs.sw.siemens.com/en-US/doc/226870983/PL20200227072959152.userGuide_pdf_2020.1/?audience=external
46. Porziani S et al (2021) Automatic shape optimisation of structural parts driven by BGM and RBF mesh morphing. *Int J Mech Sci* 189:105976
47. Papoutsis-Kiachagias EM, Porziani S, Groth C, Biancolini ME, CostaE, Giannakoglou KC (2019) Aerodynamic optimization of car shapes using the continuous adjoint method and an RBF morpher. *Advances in Evolutionary and Deterministic Methods for Design, Optimization and Control in Engineering and Sciences* 173–187
48. Kurtulus K et al (2021) An experimental investigation of the cooling and heating performance of a gravity die casting mold with conformal cooling channels. *Appl Therm Eng* 194:117105
49. Feng S, Kamat AM, Pei Y (2021) Design and fabrication of conformal cooling channels in molds: review and progress updates. *Int J Heat Mass Transf* 171:121082
50. Zeng T, Abo-Serie EF, Jewkes J, Dodd P, Jones R (2022) Adjoint method for the optimisation of conformal cooling channels of 3-D printed high-pressure tools for aluminium Casting. *SAE International Journal of Advances and Current Practices in Mobility* 4(2022-01-0246):2379–2388
51. Kan M, Ipek O (2021) A numerical and experimental investigation of the thermal behaviour of a permanent metal mould with a conventional cooling channel and a new cooling channel design. *Int J Metalcast*. <https://doi.org/10.1007/s40962-021-00633-4>
52. Coranic T, Gaspar S, Pasko J (2020) Utilisation of optimisation of internal topology in manufacturing of injection moulds by the DMLS technology. *Appl Sci* 11(1):262

Publisher's note Springer Nature remains neutral with regard to jurisdictional claims in published maps and institutional affiliations.